Spatially localized magnetoconvection

D Lo Jacono[1,2], A Bergeon[1,2] and E Knobloch[3]

[1] Université de Toulouse; INPT, UPS; Institut de Mécanique des Fluides de Toulouse (IMFT), Allée Camille Soula, F-31400 Toulouse, France
[2] CNRS, IMFT, F-31400 Toulouse, France
[3] Department of Physics, University of California, Berkeley, CA 94720, USA

E-mail: lojacono@imft.fr, bergeon@imft.fr and knobloch@berkeley.edu

Abstract

Numerical continuation is used to compute branches of time-independent, spatially localized convectons in an imposed vertical magnetic field focusing on values of the Chandrasekhar number Q in the range $10 < Q < 10^3$. The calculations reveal that convectons initially grow by nucleating additional cells on either side, but with the build-up of field outside owing to flux expulsion, the convectons are able to transport more heat only by expanding the constituent cells. Thus, at large Q and large Rayleigh numbers, convectons consist of a small number of broad cells.

1. Introduction

Convectons are spatially localized regions of convection embedded in a quiescent background. States of this type were found in numerical studies of magnetoconvection, i.e. convection in an imposed vertical magnetic field, in both two (Blanchflower 1999) and three spatial dimensions (Blanchflower and Weiss 2002, Houghton and Bushby 2011), although there is evidence for similar states in earlier work on two-dimensional (2D) natural convection in a vertical slot (Ghorayeb and Mojtabi 1997). The existence and stability of these structures have elicited considerable interest in recent years (Knobloch 2008). In a recent paper, Lo Jacono *et al* (2011) used numerical continuation to compute branches of 2D magnetohydrodynamic convectons in a periodic domain with stress-free, fixed temperature boundary conditions at the top and bottom of a horizontal layer of a conducting Boussinesq fluid, focusing on the case $Q = 4$, where the Chandrasekhar number Q provides a dimensionless measure of the strength of the imposed magnetic field. This relatively small value was selected since in this case no overstability is present for the values of the magnetic Prandtl number ($\zeta = 0.1$ and $\zeta = 0.5$) used in the computations. These values of ζ bracket the transition from subcritical to supercritical periodic convection, and allowed us to study the changes in the properties

of magnetohydrodynamic convectons as the interval of coexistence between the conduction state and spatially periodic convection shrinks and eventually disappears. In contrast to other convecton-bearing systems Lo Jacono *et al* (2011) found that the convectons persisted into the supercritical regime and, following Cox and Matthews (2001), attributed this fact to the presence of a conserved quantity, the imposed magnetic flux.

In this paper, we use the same procedure to extend the results of Lo Jacono *et al* (2011) to larger values of Q. Specifically, we report here on the results obtained for (i) $Q = 100$, (ii) $Q = 400$ and (iii) $Q = 1000$, all with $\zeta = 0.5$ and $\sigma = 1$, where σ denotes the Prandtl number. For this parameter choice, the width of the diffusive boundary layers, measured by the Péclet and magnetic Reynolds numbers $Pe \equiv Uh/\kappa$, $Re_{\mathrm{m}} \equiv Uh/\eta$, remains of order h, the layer depth, provided that the imposed Rayleigh number Ra remains of order Ra_{c}, the critical Rayleigh number for the onset of convection. Here κ and η are the thermal and ohmic diffusivities and U denotes a characteristic convective speed. However, with increasing values of Ra the boundary layers become thinner and thinner, leading to a substantial increase in the resolution requirements of our spectral element continuation code (Assemat *et al* 2008, Bergeon and Knobloch 2008). All our computations are carried out in a periodic domain with aspect ratios $\Gamma = 10\lambda_{\mathrm{c}}$ or $\Gamma = 20\lambda_{\mathrm{c}}$, where λ_{c} is the convection wavelength at $Ra = Ra_{\mathrm{c}}$.

The larger values of Q considered here are responsible for two important differences from the $Q = 4$ case considered by Lo Jacono *et al* (2011). Specifically, the onset of steady convection is delayed to larger values of Ra although the bifurcation to steady convection remains supercritical (see equation (10)). In addition, the onset of steady convection is preceded by a number of Hopf bifurcations to modes with other horizontal wavenumbers. We do not compute the resulting branches of standing and traveling waves; see Weiss (1981), Knobloch and Proctor (1981), Knobloch *et al* (1981), and Dangelmayr and Knobloch (1986) for further discussion. Owing to the cost involved we do not continue the eigenvalues describing the stability of the convectons, but expect, following Blanchflower (1999), that the solutions we compute will be stable in the vicinity of the minimum Rayleigh number for the existence of convectons. As discussed further below, this Rayleigh number is a strong function of the length of the domain used for the computations. This is in turn a consequence of the conservation of magnetic flux across the layer.

Convection in an imposed magnetic field is described by the dimensionless equations

$$\boldsymbol{u}_t + (\boldsymbol{u}\cdot\boldsymbol{\nabla})\boldsymbol{u} = -\boldsymbol{\nabla} P + \sigma Ra T\hat{\mathbf{z}} + \sigma\zeta Q(\boldsymbol{\nabla}\times\mathbf{B})\times\mathbf{B} + \sigma\nabla^2\boldsymbol{u}, \tag{1}$$

$$T_t + (\boldsymbol{u}\cdot\boldsymbol{\nabla})T = \nabla^2 T, \tag{2}$$

$$\mathbf{B}_t + (\boldsymbol{u}\cdot\boldsymbol{\nabla})\mathbf{B} = (\mathbf{B}\cdot\boldsymbol{\nabla})\boldsymbol{u} + \zeta\nabla^2\mathbf{B}, \tag{3}$$

together with the incompressibility condition

$$\boldsymbol{\nabla}\cdot\boldsymbol{u} = 0. \tag{4}$$

Here $\boldsymbol{u}$ is the velocity, P is the pressure, T is the temperature and $\mathbf{B}$ is the magnetic field, and the equations have been nondimensionalized with respect to the thermal diffusion time h^2/κ in the vertical. The system is characterized by four dimensionless parameters, the Rayleigh number $Ra \equiv \alpha\Delta T h^3/\kappa\nu$ measuring the strength of the thermal forcing (i.e. temperature difference ΔT), the Chandrasekhar number $Q \equiv B_0^2 h^2/\mu_0\rho\eta\nu$ measuring the strength of the ambient magnetic field B_0 and the two Prandtl numbers $\sigma = \nu/\kappa$ and $\zeta = \eta/\kappa$. Here ν is the kinematic viscosity.

In two dimensions it is convenient to rewrite these equations in terms of the temperature departure θ from the conduction profile, $T = 1 - z + \theta$, and the flow-induced magnetic field

perturbation $\mathbf{b}$ from the imposed vertical field, $\mathbf{B} = \hat{\mathbf{z}} + \mathbf{b}$. With $\boldsymbol{u} \equiv \boldsymbol{\nabla} \times \psi\hat{\mathbf{y}}$ and $\mathbf{b} \equiv \boldsymbol{\nabla} \times A\hat{\mathbf{y}}$ these equations take the form

$$\nabla^2\psi_t + J(\psi, \nabla^2\psi) = \sigma Ra\theta_x + \sigma\zeta Q J(x + A, \nabla^2 A) + \sigma\nabla^4\psi, \tag{5}$$

$$\theta_t + J(\psi, \theta) = \psi_x + \nabla^2\theta, \tag{6}$$

$$A_t + J(\psi, A) = \psi_z + \zeta\nabla^2 A. \tag{7}$$

We study these equations with stress-free fixed temperature boundary conditions

$$\psi = \psi_{zz} = \theta = 0 \quad \text{on } z = 0, 1, \tag{8}$$

and for the magnetic field we take the force-free boundary conditions

$$A_z = 0 \quad \text{on } z = 0, 1. \tag{9}$$

In addition, we impose periodic boundary conditions in the horizontal with period Γ. With these boundary conditions the quantity $\bar{A} \equiv \Gamma^{-1}\int_0^\Gamma \int_0^1 A(x, z, t)\, \mathrm{d}x\, \mathrm{d}z$ remains constant in time.

These equations have a trivial homogeneous solution $(\psi, \theta, A) = (0, 0, 0)$ corresponding to pure thermal conduction. Linear stability theory shows that this state loses stability with respect to exponentially growing disturbances with wavenumber k when Ra reaches $Ra(k) = (p^3/k^2)[1 + (\pi^2/p^2)Q]$, where $p \equiv \pi^2 + k^2$. The critical Rayleigh number $Ra_c \equiv Ra(k_c)$ and the wavenumber k_c of the critical disturbance are obtained by minimizing the onset Rayleigh number with respect to k. Neither depends on the parameters ζ and σ. Classical theory shows that at $Ra = Ra_c$ a steady-state bifurcation creates a branch of spatially periodic states with wavenumber k_c (equivalently, wavelength λ_c) that bifurcates subcritically when

$$1 + \frac{\pi^2}{p^2}\left[1 + \frac{2\pi^2(p - 2\pi^2)}{p(p - \pi^2)}\frac{1}{\zeta^2}\right]Q < 0 \tag{10}$$

and supercritically otherwise (Weiss 1981, Knobloch *et al* 1981). Moreover, when condition (10) holds and the problem is formulated on the real line, this instability gives rise, in addition, to two families of subcritical branches of spatially localized states of opposite parity under reflection in a vertical plane through their midpoint. Each solution type can, in addition, be reflected in the layer midplane and/or translated horizontally to generate other members of each family (Lo Jacono *et al* 2010, Mercader *et al* 2011).

We mention that the conduction state loses stability with respect to oscillations at $Ra(k) = \sigma^{-1}(p^3/k^2)(\sigma + \zeta)[(1 + \zeta) + \sigma\zeta(\pi^2/p^2)Q/(1 + \sigma)]$, a quantity that is minimized by taking $k = k_H$. The corresponding Rayleigh number and oscillation frequency will be referred to as Ra_H, ω_H, respectively, where $\omega_H^2 = (p_H/k_H^2)[-\zeta^2 + (1 - \zeta)\sigma\zeta(\pi^2/p_H^2)Q/(1 + \sigma)]$.

2. Results

2.1. $Q = 100$

For $Q = 100$, linear theory in an infinite domain yields $Ra_c \approx 2653.7$, $k_c \approx 3.7015$, independently of the value of ζ, while the first Hopf bifurcation from the conduction state occurs at $Ra = Ra_H \approx 2429.2$, with critical wavenumber $k_H \approx 2.7561$ and frequency $\omega_H \approx 6.8636$. Since $\Gamma = 10\lambda_c$, where $\lambda_c \equiv 2\pi/k_c$, the steady-state instability sets in at $Ra = Ra_c$ and gives rise to a (supercritical) spatially periodic state we call P_{10}, consisting of 20 counter-rotating rolls per period Γ. The steady, spatially localized, states of interest here bifurcate from this state in a secondary bifurcation that takes place already at small amplitude.

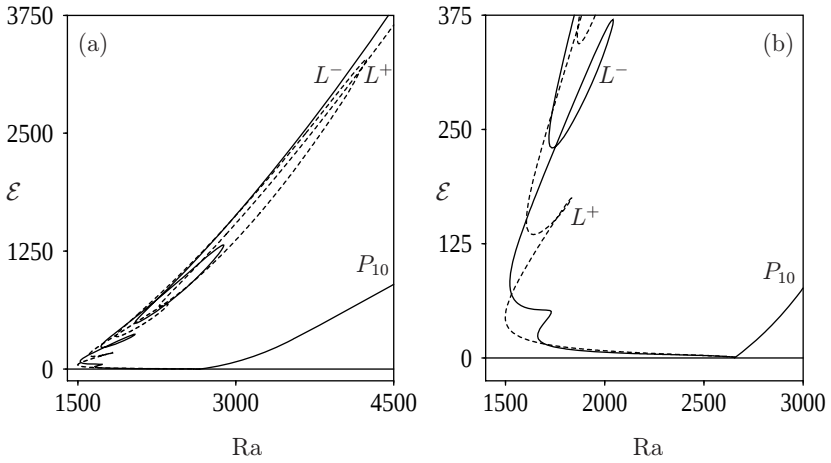

Figure 1. (a) Bifurcation diagram for $Q = 100$ in a $\Gamma = 10\lambda_c$ domain showing the energy $\mathcal{E}$ as a function of the Rayleigh number Ra for the periodic branch P_{10} and the branches of even (L^+, dashed line) and odd (L^-, solid line) parity convectons. (b) Enlargement of (a).

Figure 1 shows the kinetic energy $\mathcal{E} \equiv (1/2)\int_0^\Gamma \int_0^1 |\boldsymbol{u}|^2 \, \mathrm{d}x \, \mathrm{d}z$ as a function of the Rayleigh number Ra for the periodic state P_{10}, together with a pair of spatially localized states of even (L^+, dashed line) and odd (L^-, solid line) parity. This representation does not distinguish between states related by reflection symmetry in the midplane or by translations. The P_{10} solutions undergo a secondary bifurcation already at small amplitude through an instability first identified by Matthews and Cox (2000). This bifurcation is strongly subcritical and generates two pairs of branches of opposite-parity spatially localized structures (figure 1(b)), exactly as in the case $Q = 4$ (Lo Jacono *et al* 2011). These branches are initially exponentially close and the corresponding structures are weakly localized and unstable. However, with increasing amplitude (decreasing Ra) the structures rapidly localize before turning around in saddle node bifurcations and beginning to grow in length by nucleating new convection cells at either end. In the following, we denote the leftmost saddle node on each branch by $Ra = Ra^*_{\mathrm{odd/even}}$.

During this growth process the midplane magnetic potential $A(x, z = 1/2)$ develops a nonzero slope which remains almost constant in the center of the structure despite the changing Rayleigh number and the growing number of rolls on either side. The rolls imprint a staircase structure on this overall slope, by an essentially kinematic flux expulsion process elucidated by Weiss (1966), and the overall appearance of $A(x, z = 1/2)$ is almost identical for both even and odd states. This is a consequence of the fact that the cells expel magnetic field regardless of their direction of rotation. Thus a churning array of cells expels field to the boundary of the array regardless of whether the outermost cells rotate in the same or opposite directions. The mean slope of $A(x, 1/2)$ represents reduction (negative slope) in the vertical magnetic field within the structure and enhancement (positive slope) outside (figures 2 and 3). Thus the resulting vertical magnetic field has an essentially piecewise constant profile: reduced within the structure, except at cell boundaries, and enhanced outside.

The growth process manifests itself in a series of loops in $\mathcal{E}$ as R increases (figure 1). These loops are associated with the nucleation of additional cells as the number of cells within the convecton grows (figures 2 and 3). The origin of the loops themselves can be traced to a gradual increase in the wavelength of the cells within the convecton as Ra increases—such

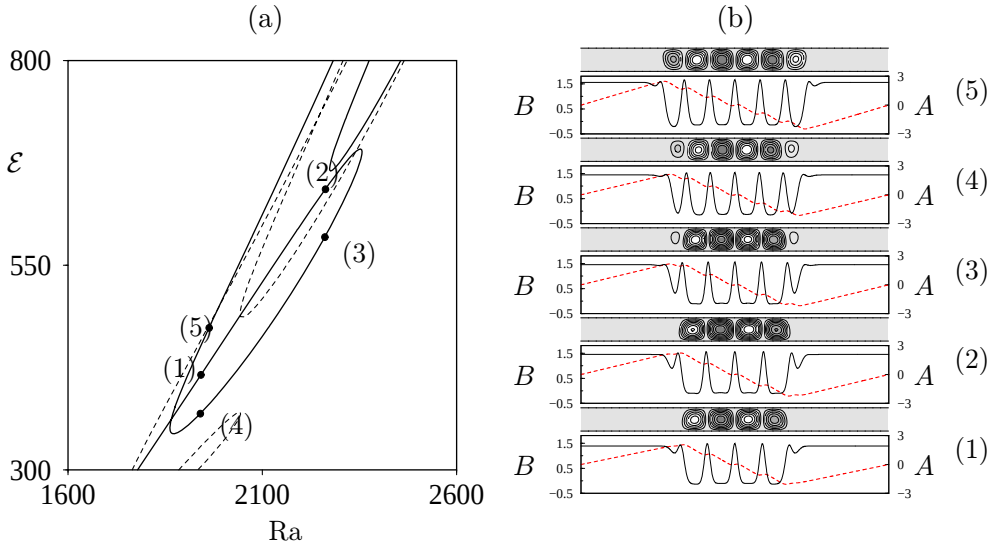

Figure 2. (a) Bifurcation diagram for $Q = 100$ in a $\Gamma = 10\lambda_c$ domain showing details of the loop structure in figure 1 for even (solid line) and odd (dashed line) convectons. (b) Even parity convectons at the locations indicated in (a). Top panels: contours of the streamfunction $\psi(x, z)$. Bottom panels: the magnetic potential $A(x, 1/2)$ (dashed profile) and the corresponding vertical magnetic field $B(x, 1/2) \equiv 1 + A_x(x, 1/2)$ (solid profile), both at midplane $z = 1/2$.

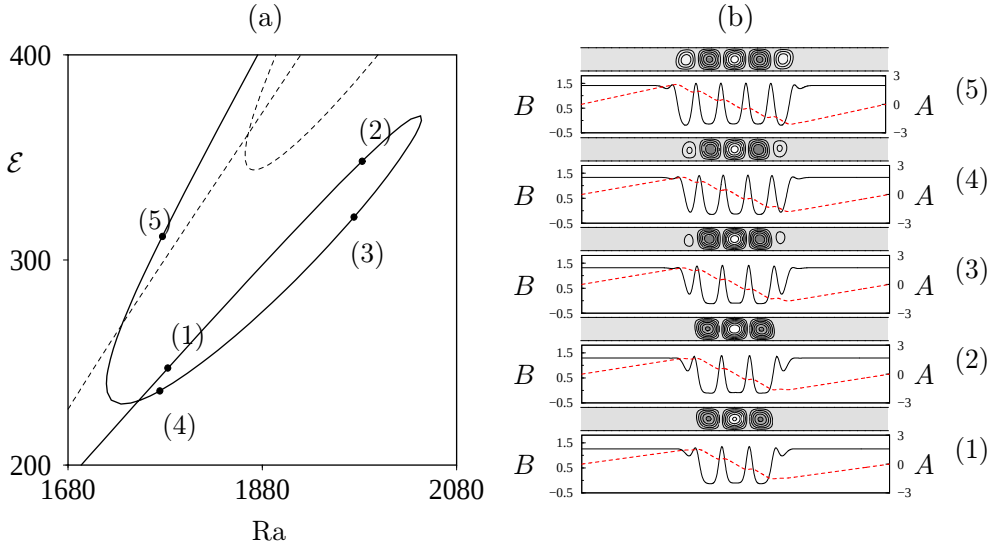

Figure 3. (a) Bifurcation diagram for $Q = 100$ in a $\Gamma = 10\lambda_c$ domain showing details of the loop structure in figure 1 for odd (solid line) and even (dashed line) convectons. (b) Odd parity convectons at the locations indicated in (a). Top panels: contours of the streamfunction $\psi(x, z)$. Bottom panels: the magnetic potential $A(x, 1/2)$ (dashed profile) and the corresponding vertical magnetic field $B(x, 1/2) \equiv 1 + A_x(x, 1/2)$ (solid profile), both at midplane $z = 1/2$.

an increase is possible because the convectons are localized—followed by a decrease in wavelength once new cells nucleate at a saddle node on the right (figures 2 and 3). It is as if the new cells, one on each side, squeeze the convecton between them. This effect grows as the new

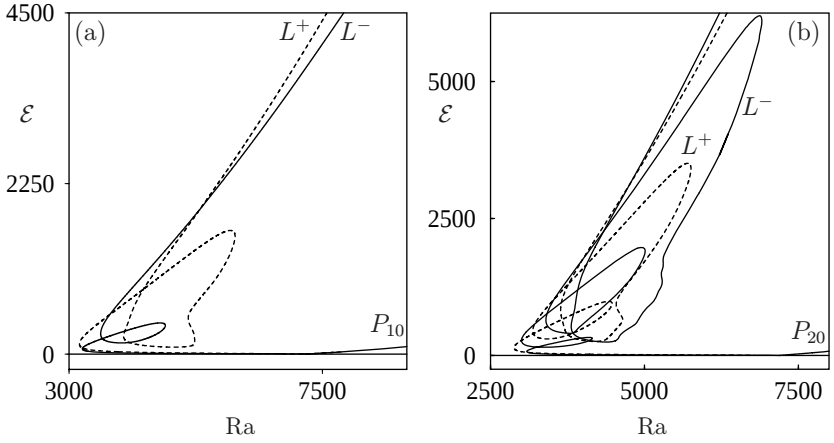

Figure 4. Bifurcation diagram for $Q = 400$ in a (a) $\Gamma = 10\lambda_c$, (b) $\Gamma = 20\lambda_c$ domain showing the energy $\mathcal{E}$ as a function of the Rayleigh number Ra for the periodic branch P_{10} (P_{20}) and the branches of even (L^+, dashed line) and odd (L^-, solid line) parity convectons.

cells grow to their saturated amplitude, a process that takes place along the lower portion of each loop. Beyond the saddle node on the left all the cells within the convecton are of the same strength and the wavelength starts to increase again. Thus, despite the increase in the number of cells the convectons along the lower portion of each loop are shorter and hence occupy a smaller fraction of the domain than prior to the nucleation event, resulting in decreased kinetic energy $\mathcal{E}$ (figures 2 and 3). This process repeats as Ra increases with the loops getting larger as the associated changes in energy become larger, before the domain is full. Once enough space is not available to insert new cells on either side, the structure ceases to grow, and only the vigor of the convecting cells increases with further increase in Ra (figure 1(a)). The resulting states resemble the defect states studied elsewhere (Bergeon and Knobloch 2008, Mercader *et al* 2009) and the resulting structure resembles slanted snaking (Firth *et al* 2007, Dawes 2008).

2.2. $Q = 400$

With increasing Q the number of loops gradually decreases. For example, when $\Gamma = 10\lambda_c$ and $Q = 250$ (not shown) only two loops are present on each convecton branch, while only one is present when $Q = 400$ (figure 4(a)). This fact implies a dramatic change in the convecton growth process since the presence of loops indicates nucleation of new cells. Thus the convecton must manage to transport more and more heat as the Rayleigh number increases without adding new cells. To see how this is possible we now present the results for $Q = 400$. For this value of Q linear theory yields $Ra_c \approx 7185.9$, $k_c \approx 4.7942$, independently of the value of ζ, while the first Hopf bifurcation from the conduction state occurs already at $Ra = Ra_H \approx 4658.9$, with critical wavenumber $k_H \approx 3.4395$ (for $\zeta = 0.5$, $\sigma = 1$).

Figures 5 and 6 show that for $Q = 400$ the vertical magnetic field, $B(x, 1/2)$, has a more nonlinear, square-wave profile in the saturated state. Indeed, the profiles are no longer monotonic and the slight dips on either side of an upflow or a downflow are the result of advection of the field by the rising or falling plume. A careful examination of the solution profiles along the remaining loop reveals that the wavelength is no longer selected by the value of Ra alone. Instead figures 5 and 6 reveal a significant dependence on the

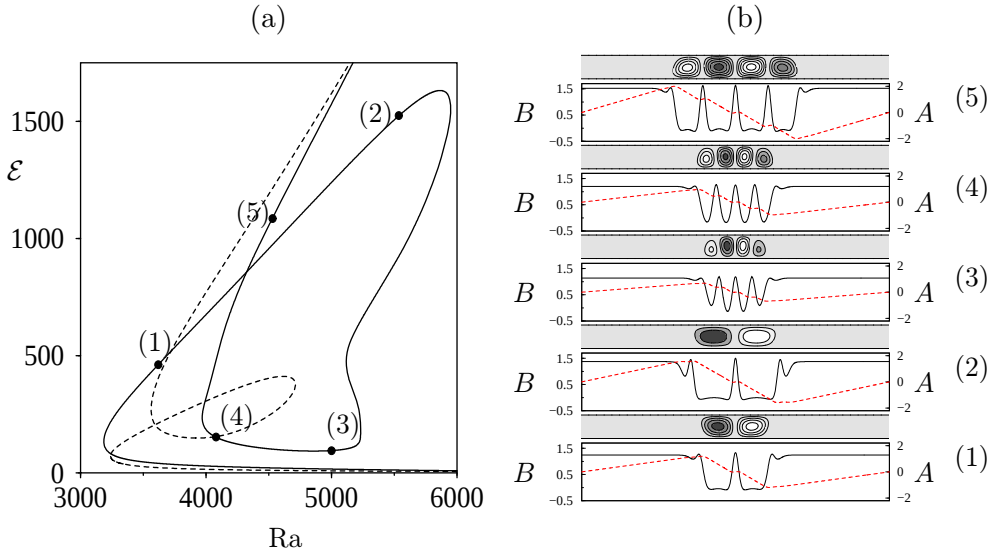

Figure 5. (a) Bifurcation diagram for $Q = 400$ in a $\Gamma = 10\lambda_c$ domain showing details of the loop structure in figure 4(a) for even (solid line) and odd (dashed line) convectons. (b) Even parity convectons at the locations indicated in (a). Top panels: contours of the streamfunction $\psi(x, z)$. Bottom panels: the magnetic potential $A(x, 1/2)$ (dashed profile) and the corresponding vertical magnetic field $B(x, 1/2) \equiv 1 + A_x(x, 1/2)$ (solid profile), both at midplane $z = 1/2$.

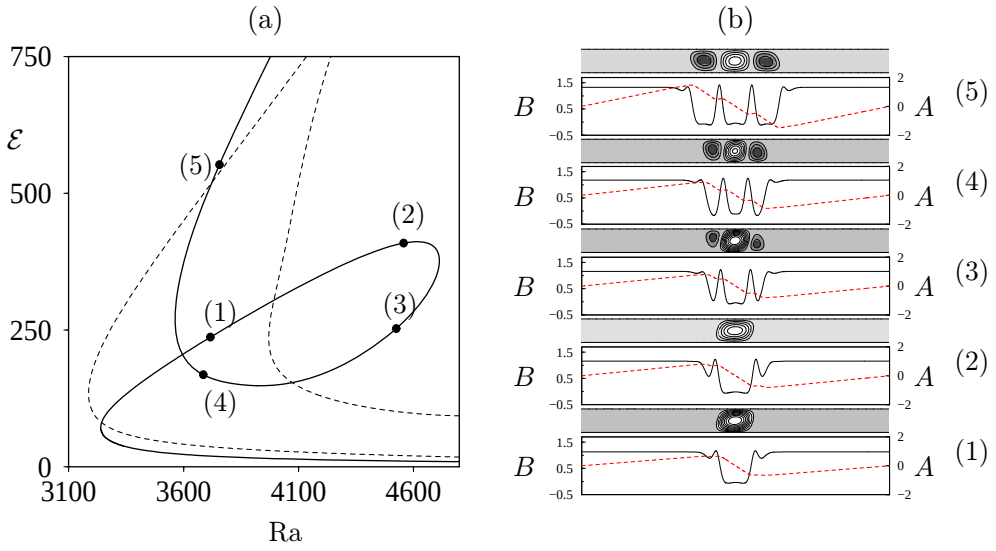

Figure 6. (a) Bifurcation diagram for $Q = 400$ in a $\Gamma = 10\lambda_c$ domain showing details of the loop structure in figure 4(a) for odd (solid line) and even (dashed line) convectons. (b) Odd parity convectons at the locations indicated in (a). Top panels: contours of the streamfunction $\psi(x, z)$. Bottom panels: the magnetic potential $A(x, 1/2)$ (dashed profile) and the corresponding vertical magnetic field $B(x, 1/2) \equiv 1 + A_x(x, 1/2)$ (solid profile), both at midplane $z = 1/2$.

amplitude of state, with the low-energy state having a substantially shorter wavelength than the large-amplitude states even at comparable Rayleigh numbers. The figures also reveal a considerable dependence of the flux expulsion process on the amplitude of the localized

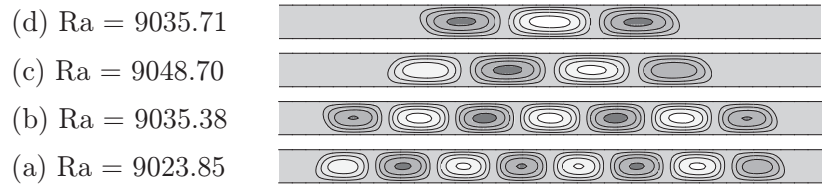

Figure 7. Profiles for even and odd convectons for (a–b) $Q = 100$, $\Gamma = 10\lambda_c$ and (c–d) $Q = 400$, $\Gamma = 10\lambda_c$ at the Rayleigh numbers indicated, showing large wavelength nearly periodic structures filling the domain at large Ra when Q is also large.

structures, as measured by the slope of $A(x, z = 1/2)$ outside the structure (dashed profiles), with fully developed convectons much more efficient at flux expulsion. This is primarily the consequence of a larger magnetic Reynolds number Re_m. The increased magnetic field outside the convecton in turn suppresses the nucleation of new cells and leads to a new growth process as Ra increases. Thus flux conservation leads to suppression of nucleation. For $Q = 400$ this occurs after the even convecton has grown to four cells and the odd convecton to three cells (figures 5 and 6) as expected from the presence of a single loop on each branch. Instead one finds that beyond the loop the width of the individual cells in each of these states begins to increase monotonically with increasing Ra until the domain is almost full. This new growth process thus results in a cellular state with a relatively large wavelength (figure 7), with defects or holes separated by distance Γ.

To confirm this picture we have recomputed our $Q = 400$ results on a domain with $\Gamma = 20\lambda_c$. Figure 4(b) shows the presence of two loops on the branch of even convectons and three loops on the branch of odd convectons instead of one loop on each branch, and indeed the convectons now consist of six cells (even) or seven cells (odd) when the loops cease and the existing cells start to stretch (not shown). These results confirm that the transition from nucleation of new cells to the stretching of existing cells is triggered by a critical strength of the ambient magnetic field.

In figure 7, we compare the large Rayleigh number $Q = 400$, $\Gamma = 10\lambda_c$ solutions with the corresponding solutions for $Q = 100$, $\Gamma = 10\lambda_c$. We see that the wavelength of the structure when $Q = 400$ is much larger than when $Q = 100$ but that it remains uniform even at $Ra \sim 9000$. At these large values of Ra the solution branches increase monotonically, much as in figure 4(a), with no additional features.

2.3. $Q = 1000$

For $Q = 1000$ linear theory yields $Ra_c \approx 15207$, $k_c \approx 5.6842$, independently of the value of ζ, while the first Hopf bifurcation from the conduction state occurs already at $Ra = Ra_H \approx 8415.3$, with critical wavenumber $k_H \approx 4.0691$ (for $\zeta = 0.5$, $\sigma = 1$).

For this large value of Q the behavior of the convecton branches $L_{10}^{\pm}$ and $L_{20}^{\pm}$ is considerably different (figure 8). The regular looping seen at smaller values of Q is now absent and there are substantial differences in the behavior of the odd and even convectons. The results are also sensitive to the domain length Γ with the leftmost saddle nodes shifting towards smaller Rayleigh numbers as the domain increases. This is again a consequence of flux conservation. On smaller domains flux conservation increases the magnetic field strength outside the convecton, thereby limiting convection to larger Rayleigh numbers than in larger domains. Thus for large Q the first saddle node for odd convections is further to the left than for even convectons.

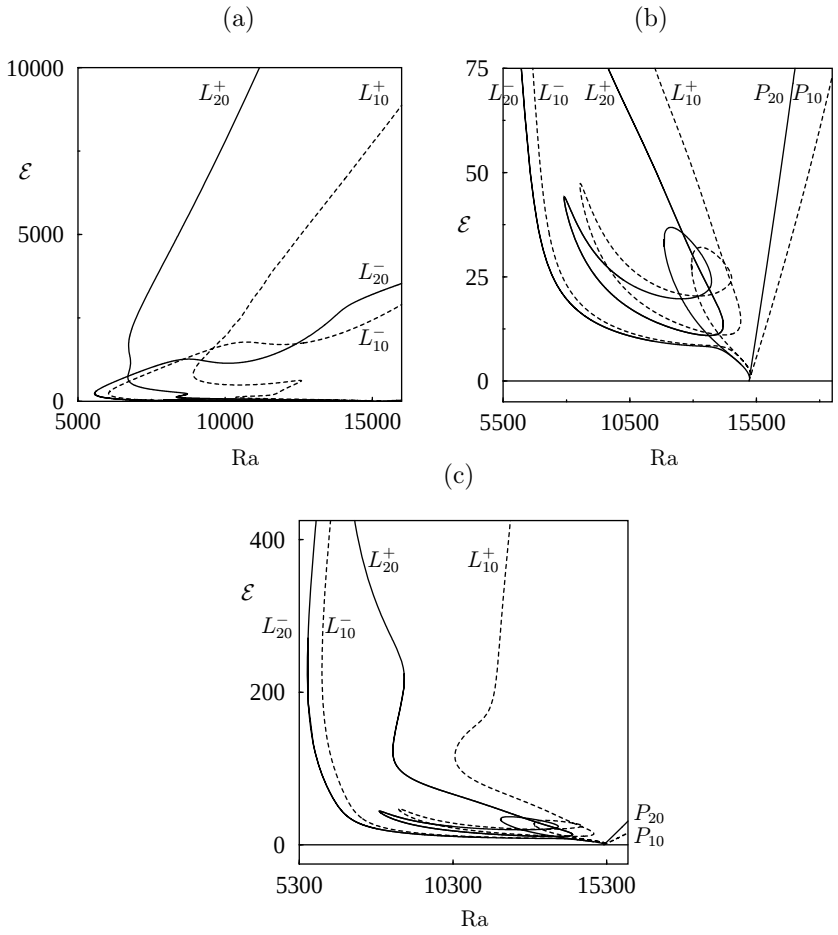

Figure 8. (a) Bifurcation diagram for $Q = 1000$ in a $\Gamma = 10\lambda_c$ domain (dashed curves) and a $\Gamma = 20\lambda_c$ domain (solid curves) showing the energy $\mathcal{E}$ as a function of the Rayleigh number Ra for the periodic branches P_{10} and P_{20} and the branches of even and odd parity convectons $L_{10}^{\pm}$ and $L_{20}^{\pm}$. (b) Enlargement of (a) near the primary bifurcation. (c) Enlargement of (a) on an intermediate scale, below the leftmost saddle nodes on the L_{10}^{+} and L_{20}^{+} branches.

Figure 9 shows sample solutions at the left saddle nodes along (a) L_{20}^{+} and (b) L_{20}^{-} in a $\Gamma = 20\lambda_c$ domain. As shown in figure 8(b) the L_{20}^{+} branch goes through a loop at small amplitude after which the solution consists of four cells. However, near the spike that follows (this spike is clearly visible in figure 8(b)), the even parity solution briefly splits into a bound state of two oppositely oriented single-cell convectons before recombining into a four-cell state in which the outer cells retain their dominance. With increasing amplitude (figure 8(c)) the inner cells grow in both amplitude and wavelength, forming, by the time the leftmost saddle node is reached, a state consisting of four similar cells. At this point the cells start to stretch, resulting in the four-cell state shown in figure 9(a) at $Ra = 12\,187$. In contrast to the even parity states, the energy of the odd parity states L_{20}^{-} grows much more slowly (figure 9(b)). These states undergo only a single saddle node at which the solution takes the form of a single convecting cell. With increasing amplitude the branch L_{20}^{-} turns around and the solution gradually adds narrow convection cells on either side, without exhibiting either

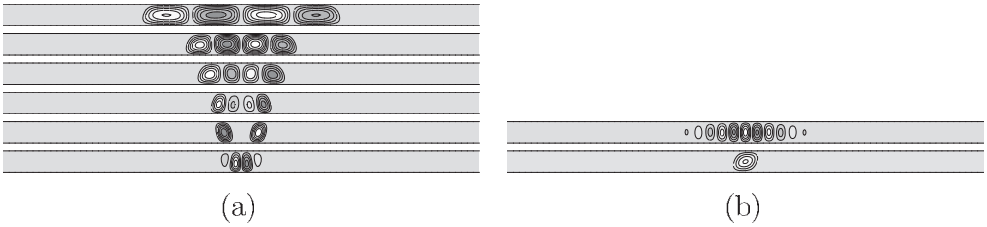

Figure 9. Solutions when $Q = 1000$, $\Gamma = 20\lambda_c$. (a) Streamfunction at left saddle nodes along the L_{20}^{+} branch ($Ra \approx 11\,880$, 7906, 8360, 6701, 6717) and at large Ra ($Ra = 12\,187$). (b) Streamfunction at the left saddle node along the L_{20}^{-} branch ($Ra \approx 5612$), and at large Ra ($Ra = 15\,039$). In each case the kinetic energy $\mathcal{E}$ increases from the bottom to the top.

additional loops or additional saddle nodes. This behavior, already seen when $Q = 4$ (Lo Jacono *et al* 2011), resembles the 'smooth snaking' first described in the context of a nonlocal oscillon model by Dawes and Lilley (2010). The resulting solution, shown in figure 9(b) at $Ra = 15\,039$, resembles the narrow convection cells traditionally expected of convection in a strong magnetic field (Julien *et al* 1999, Matthews 1999), but differs dramatically from the corresponding large-amplitude even state in figure 9(a).

2.4. Location of the leftmost saddle nodes

In figure 10, we show the location of the leftmost saddle nodes, $Ra = Ra^{*}_{\mathrm{odd/even}}$, on the branches of odd and even convectons for different values of Q in the range $100 \leqslant Q \leqslant 1000$ computed for $\Gamma = 20\lambda_c$. The states corresponding to these saddle nodes are well-localized convectons consisting of one or two cells only. In contrast to the suggestion of Dawes (2007) based on the results in domains with $\Gamma = 6$ and $\Gamma = 10$, i.e. for substantially smaller domains than in this work, we do not see a Γ-independent power law dependence on Q. Our computations suggest (figure 8) that the location of the leftmost saddle nodes is in fact a sensitive function of the aspect ratio Γ even for the relatively large domains employed in our computations. This is a consequence of flux conservation, which plays a fundamental role in finite domains even for nominally localized structures (Lo Jacono *et al* 2011). Despite this difference we expect to find *stable* convectons above and close to the saddle node lines shown in the figure, as found by Blanchflower (1999) and confirmed by Dawes (2007) using direct numerical simulations.

3. Discussion

In this paper, we have extended the results obtained by Lo Jacono *et al* (2011) for magnetoconvection with $Q = 4$ to substantially larger values of Q. In order to reduce resolution requirements we used the magnetic Prandtl number $\zeta = 0.5$ and considered periodic domains $\Gamma = 10\lambda_c$ and $\Gamma = 20\lambda_c$ with 10 and 20 critical wavelengths, respectively. For these parameter values the periodic state bifurcates supercritically. Despite this, spatially localized states of odd and even parity are present for Rayleigh numbers below $Ra = Ra_c$, indeed substantially below $Ra = Ra_c$. Although we have presented detailed results only for $Q = 100$, 400 and 1000 we have performed similar computations for a range of values of Q in the range $10 \leqslant Q \leqslant 1000$. These suggest that there are two qualitatively distinct types of behavior. For $10 \leqslant Q \leqslant 100$ the system behaves much as shown in figures 1–3 with orderly growth of the localized structure that manifests itself in the presence of loops in the

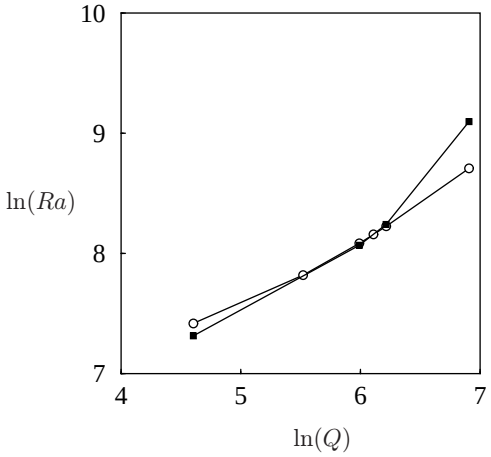

Figure 10. The location in a log–log plot of the leftmost saddle nodes $Ra = Ra^*_{\mathrm{even}}$ for even convectons (open circles) and $Ra = Ra^*_{\mathrm{odd}}$ for odd convectons (solid squares) as functions of Q, computed with $\Gamma = 20\lambda_c$.

energy $\mathcal{E}$. In this regime the effects of flux conservation are limited to the regime in which the convectons almost fill the entire domain (figures 7(a) and (b)). For larger Q these loops gradually disappear, as the build-up of the magnetic field outside the structure suppresses the nucleation of new cells on either side. We conjectured that in larger domains the suppression of nucleation will be delayed until the ambient magnetic field reaches the strengths at which nucleation is suppressed in domains with aspect ratio $\Gamma = 10\lambda_c$. This conjecture is confirmed in figure 4(b), which reveals the presence of three loops when $\Gamma = 20\lambda_c$, all other parameters remaining the same. Beyond this point the cells must broaden in order to carry the heat that is supplied.

The appearance of broader cells within the convectons as Q increases shows that extrapolation of linear theory predictions to strongly nonlinear solutions is dangerous—linear theory predicts that the wavelength of convection cells varies with Q as $Q^{-1/6}$ and hence that cells become narrower as the magnetic field strength increases. For the largest magnetic field strengths examined, $Q = 1000$, we found narrow cell convectons at large Rayleigh numbers to be of odd parity only, with the corresponding even parity states consisting of a small number of broad cells. It is possible, but remains unproven, that for still larger values of Q these broad cell states undergo a transition to narrow cells with a concomitant decrease in slope of $\mathcal{E}(Ra)$ owing to increased viscous dissipation.

Based on earlier results with $Q = 4$ we conjecture that similar results to those reported here will be obtained for smaller values of the diffusivity ratio ζ. For $\zeta \ll 1$ the bifurcation to periodic convection becomes strongly subcritical but since the convectons reported here are already strongly subcritical we anticipate little qualitative effect on these states. However, since the magnetic boundary layers become thinner and thinner as ζ decreases, we expect flux expulsion to be more complete at any given Rayleigh number, and hence expect the leftmost saddle nodes to shift to yet smaller values of Ra.

Acknowledgments

This work was supported in part by the National Science Foundation under grant no DMS-0908102. We have benefitted from discussions with H-C Kao.

References

Assemat P, Bergeon A and Knobloch E 2008 Spatially localized states in Marangoni convection in binary mixtures *Fluid Dyn. Res.* **40** 852–76

Bergeon A, Burke J, Knobloch E and Mercader I 2008 Eckhaus instability and homoclinic snaking *Phys. Rev.* E **78** 046201

Bergeon A and Knobloch E 2008 Spatially localized states in natural doubly diffusive convection *Phys. Fluids* **20** 034102

Blanchflower S 1999 Magnetohydrodynamic convectons *Phys. Lett.* A **261** 74–81

Blanchflower S and Weiss N 2002 Three-dimensional magnetohydrodynamic convectons *Phys. Lett.* A **294** 297–303

Cox S M and Matthews P C 2001 New instabilities in two-dimensional rotating convection and magnetoconvection *Physica* D **149** 210–29

Dangelmayr G and Knobloch E 1986 Interaction between standing and travelling waves and steady states in magnetoconvection *Phys. Lett.* A **117** 394–8

Dawes J H P 2007 Localized convection cells in the presence of a vertical magnetic field *J. Fluid Mech.* **570** 385–406

Dawes J H P 2008 Localized pattern formation with a large-scale mode: slanted snaking *SIAM J. Appl. Dyn. Syst.* **7** 186–206

Dawes J H P and Lilley S 2010 Localized states in a model of pattern formation in a vertically vibrated layer *SIAM J. Appl. Dyn. Syst.* **9** 238–60

Firth W J, Columbo L and Scroggie A J 2007 Proposed resolution of theory–experiment discrepancy in homoclinic snaking *Phys. Rev. Lett.* **99** 104503

Ghorayeb K and Mojtabi A 1997 Double diffusive convection in a vertical rectangular cavity *Phys. Fluids* **9** 2339–48

Houghton S M and Bushby P J 2011 Localized plumes in three-dimensional compressible magnetoconvection *Mon. Not. R. Astron. Soc.* **412** 555–60

Julien K, Knobloch E and Tobias S 1999 Strongly nonlinear magnetoconvection in three dimensions *Physica* D **128** 105–29

Knobloch E and Proctor M R E 1981 Nonlinear periodic convection in double-diffusive systems *J. Fluid Mech.* **108** 291–316

Knobloch E 2008 Spatially localized structures in dissipative systems: open problems *Nonlinearity* **21** T45–60

Knobloch E, Weiss N O and Da Costa L N 1981 Oscillatory and steady convection in a magnetic field *J. Fluid Mech.* **113** 153–86

Lo Jacono D, Bergeon A and Knobloch E 2010 Spatially localized binary fluid convection in a porous medium *Phys. Fluids* **22** 073601

Lo Jacono D, Bergeon A and Knobloch E 2011 Magnetohydrodynamic convectons *J. Fluid Mech.* **687** 595–605

Matthews P C 1999 Asymptotic solutions for nonlinear magnetoconvection *J. Fluid Mech.* **387** 397–409

Matthews P C and Cox S M 2000 Pattern formation with a conservation law *Nonlinearity* **13** 1293–320

Mercader I, Batiste O, Alonso A and Knobloch E 2009 Localized pinning states in closed containers: homoclinic snaking without bistability *Phys. Rev.* E **80** 025201

Mercader I, Batiste O, Alonso A and Knobloch E 2011 Convectons, anticonvectons and multiconvectons in binary fluid convection *J. Fluid Mech.* **667** 586–606

Weiss N O 1966 The expulsion of magnetic flux by eddies *Proc. R. Soc.* A **293** 310–28

Weiss N O 1981 Convection in an imposed magnetic field. Part 1. The development of nonlinear convection *J. Fluid Mech.* **108** 247–72